J. Phys.: Condens. Matter **20** (2008) 075107 (8pp) doi:10.1088/0953-8984/20/7/075107

Polyamorphic transitions in vitreous B_2O_3 under pressure

Liping Huang[1,4], Jason Nicholas[2,5], John Kieffer[1,6] and Jay Bass[2,3]

[1] Department of Materials Science and Engineering, University of Michigan, Ann Arbor, MI 48109, USA
[2] Department of Materials Science and Engineering, University of Illinois, Urbana, IL 61801, USA
[3] Department of Geology, University of Illinois, Urbana, IL 61801, USA

E-mail: kieffer@umich.edu

Received 24 July 2007, in final form 20 December 2007
Published 25 January 2008
Online at stacks.iop.org/JPhysCM/20/075107

Abstract

We have studied the nature of structural transitions in B_2O_3 glass under pressure using molecular dynamics simulations, based on a newly developed coordination-dependent charge transfer potential, to complement the results from our earlier Brillouin and Raman scattering experiments and to interpret these findings. This interaction model allows for charges to re-distribute between atoms upon the formation and rupture of chemical bonds, and accommodates multiple coordination states for a given species in the course of the simulation. The macroscopic observables of the simulated vitreous B_2O_3, such as the variation of density and elastic modulus with pressure, agree well with those seen in experiments. The compaction of simulated structures is based on a polyamorphic transition that involves transitory four-coordinated boron atoms at high pressures. While the coordination of boron completely reverts to trigonal upon pressure release, without this transitory coordination increase permanent densification would not be manifest in the recovered glass. The response of vitreous B_2O_3 to pressure is virtually independent of the concentration of boroxol rings in the structure. In simulated glass, boroxol rings dissolve when subject to pressure, which explains the disappearance of the breathing mode in the Raman spectrum of compressed B_2O_3 glass.

(Some figures in this article are in colour only in the electronic version)

1. Introduction

Despite being one of the archetypal network glass formers, the structure of vitreous B_2O_3 has been a much debated topic for many years, particularly with respect to the structural role played by the boroxol (B_3O_6) group. The first structural model of vitreous boron oxide proposed by Zachariasen [1] was that it consisted of a three-dimensionally random network of BO_3 triangles. This was supported by early x-ray diffraction [2] and NMR [3] studies of vitreous boron oxide. However, it was pointed out by Fajans *et al* [4] that the above random network model failed to explain many physical properties of vitreous and liquid B_2O_3. For instance, it is difficult to explain the low viscosity (at 1260 °C, the viscosity of boron oxide is smaller than that of silica by a factor $10^{-11.6}$), the low density of 1.80 g cm^{-3}, and, in light of the fact that the B–O bond is stronger than the Si–O bond, the low melting point of 450 °C for B_2O_3 [5] (silica glass has a density of 2.2 g cm^{-3} and the melting point is 1710 °C). The model of a random network of BO_3 triangles was further challenged in 1953 when an anomalously sharp and intense line was observed in the Raman spectrum of boron oxide at 808 cm^{-1} by Gorbeau *et al* [6]. The authors suggested that the BO_3 triangles were not randomly oriented, but bonded together into a boroxol (B_3O_6) ring. In 1969, Krogh-Moe [7] suggested that a three-dimensionally random network of BO_3 triangles with a comparatively high fraction of boroxol rings gave the best explanation for all the available data. The sharp 808 cm^{-1} Raman line is assigned to the symmetric stretching

[4] Present address: Department of Chemical and Biomolecular Engineering, North Carolina State University, Raleigh, NC 27695, USA.
[5] Present address: Department of Materials Science and Engineering, Northwestern University, Evanston, IL 60208, USA.
[6] Author to whom any correspondence should be addressed.

mode [8] or breathing mode [7] of the boroxol ring. Ever since, the fraction f of boron atoms that can be found in boroxol rings has been a highly debatable subject. Values of f ranging from 0.5 to 0.85 have been reported based on x-ray diffraction [9], neutron diffraction [5, 10, 11], NMR [12, 13] and Raman [14] studies. However, Dunlevey *et al* [15] argued that the fraction of boroxol rings must be small due to a discrepancy between the radial distribution function predicted for a glass with a large percentage of boroxol rings and the actual radial distribution function from their x-ray diffraction studies on hydrostatically compressed B_2O_3 glass. Soppe *et al* [16] also claimed their x-ray diffraction data can be explained very well by a model containing more or less randomly connected BO_3 triangles. Wright *et al* [17] have constructed two ball-and-stick models for B_2O_3 glass, each with equal number of boroxol groups and independent BO_3 triangles ($f = 0.75$). One model has a random arrangement of the two structural units, the other an alternate arrangement of the units. Only the random model gives correlation functions that compare favorably with neutron diffraction measurements. The density of the random model is 17% lower than that of B_2O_3 glass, suggesting that the proportion of boroxol rings is too high. Based on the physical [18] and computer generated [19] ball-and-stick model, Elliot *et al* claimed that their models did not have any boroxol rings whatsoever, but the radial distribution functions agree reasonably well with experimental curves deduced from x-ray diffraction studies. This claim has been supported by a number of molecular dynamics simulations [16, 20–25] of vitreous B_2O_3 using potentials with and without three-body constraints of the B–O–B or O–B–O angles. The aforementioned models with no boroxol rings were immediately criticized for their unrealistic bond angles (B–O–B angle is about 150°–160° in simulations compared to 130° in experiments) and their high densities. Later MD simulations, with the inclusion of three-body interactions [26–28], four-body interactions [29, 30] or many-body polarization effect [31], produced vitreous B_2O_3 glasses with fractions of boron in boroxol rings ranging from less than 1% to at most 37%. This trend is reinforced by the more recent *ab initio* [32] and reverse Monte Carlo (RMC) simulations [33, 34] suggesting that the fraction of boroxol rings ranges between 10 and 20%. The currently accepted structural model for vitreous B_2O_3 is a random mixture of BO_3 triangles and boroxol rings with no consensus on the f value.

To date, the effect of pressure on glass structure is relatively unexplored. However, since the range of pressures that can be routinely achieved in the laboratory affects large density and, implicitly, structural changes, this is a superb instrument for gaining new insights into the nature of the amorphous state of matter. In our previous simulations [35, 36], we extensively studied pressure-induced polyamorphic transitions in SiO_2 glass, a representative of a large family of four-coordinated glass-forming materials. The literature suggests that three-coordinated glasses act quite differently from four-coordinated glasses under pressure. Of the three-coordinated glasses, only As_2S_3 and B_2O_3 have been studied under pressure. Grimsditch *et al*'s early Brillouin scattering studies [37] showed that As_2S_3 follows the same sound velocity-pressure path upon compression and decompression (up to 4 GPa), whereas B_2O_3 exhibits a closed, gradual hysteresis (upon maximum compression to 15 GPa). These smooth, continuous changes are more indicative of gradual rearrangements in a random network than of a transition between structurally distinct vitreous polymorphs. In contrast, our recent concurrent Brillouin and Raman experiments [38–40] suggest that vitreous polymorphs do exist in B_2O_3 and that the transitions between vitreous polymorphs can be abrupt. Upon compression the sound velocities increase smoothly and the boroxol ring Raman mode (808 cm^{-1}) vanishes by 11 GPa. Upon decompression the sound velocities follow a different path and at 2–3 GPa exhibit a discontinuity in sound speeds of 3 km s^{-1} in V_p (longitudinal) and 2 km s^{-1} in V_s (shear), which returns the velocities to the values obtained on compression. After the transition, the boroxol ring Raman mode reappears. In addition, a new peak at 881 cm^{-1} appears in the spectrum, which to date has not definitively been assigned to a structural feature. A second pressure cycle produces the same behavior, suggesting the 2–3 GPa transition occurs between vitreous states with distinct and well-defined structures. The discontinuity at 2–3 GPa could be the result of boron going from four to three coordination based on the location of the discontinuity on the pressure scale: it occurs at a pressure close to that of the boundary between crystalline α-B_2O_3 (with three-coordinated boron) and β-B_2O_3 (with distortedly tetrahedrally coordinated boron). This speculation was supported by recent inelastic x-ray scattering (IXS) studies, which provide '*in situ*' direct experimental evidence of a reversible coordination transformation in the borate glasses under pressure [41].

It is the focus of this paper to understand the microscopic mechanism of the polyamorphic transitions in vitreous B_2O_3, i.e., the conversion between distinct local structural motifs, each sufficiently unique to define a different topology in the ensuing glassy network, as well as to validate the coordination conversion of boron under pressure. To simulate systems like boron oxide made of species that can achieve multiple coordination states, we have developed interaction models that allow coordination change during simulations [42]. In this paper we present the application of this new coordination-dependent charge transfer potential to simulating the high-pressure behavior of boron oxide glass, and, based on the comparison between simulation results and light scattering experiments, we derive new insights into the pressure-induced structural transitions in this material.

2. Potential parameters and computational procedure

A detailed description of the charge transfer three-body potential used in this study is given in [42]. For a given coordination state, the potential was parameterized by matching the simulated to experimental values of density, bond lengths and bond angles, for known crystalline polymorphs, such as B_2O_3-I and B_2O_3-II. The parameters were further adjusted to give best agreement of density, radial distribution function, structure factor, bond angle distribution, vibrational

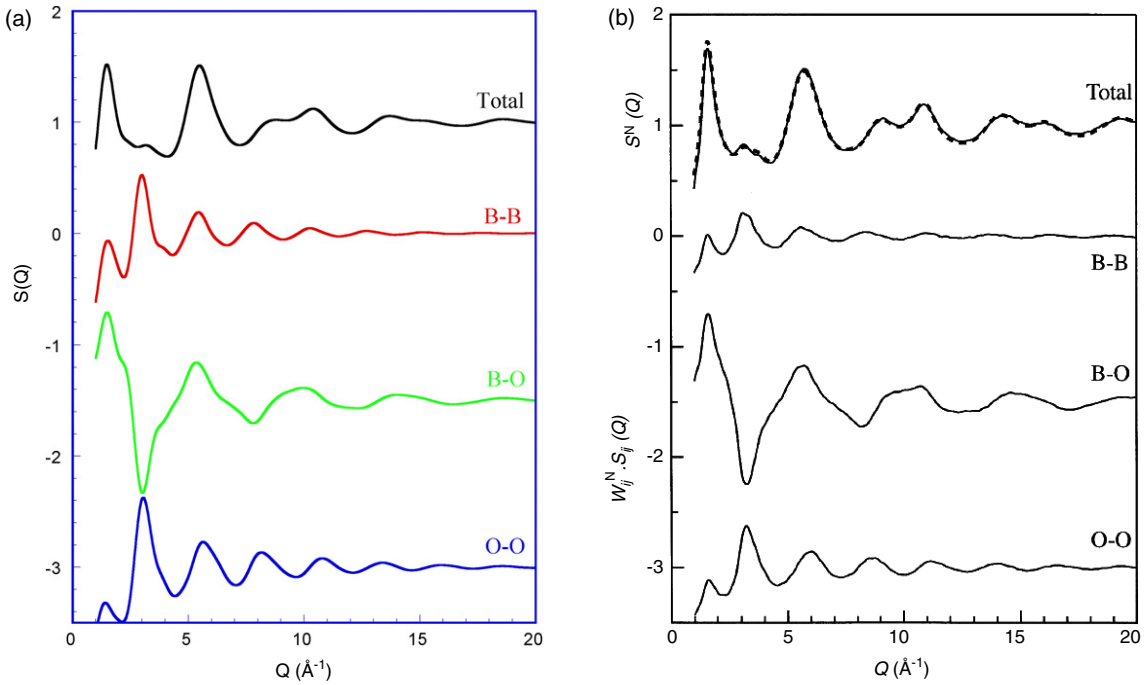

Figure 1. Total and partial structure factor $S(Q)$ from MD simulations (a) compared to those from neutron scattering experiments [34] (b).

density of states and infrared spectra of molten B_2O_3 with experimental data.

The parameters for the coordination-dependent part of the potential were adjusted so that the coordination of boron in crystalline B_2O_3-I is 3 at ambient conditions, and starts to change from 3 to 4 at approximately 3 GPa, i.e., the pressure at which B_2O_3-I transforms in B_2O_3-II in experiments. We ascertained that these parameters allow the coordination of boron to increase upon compression and return to 3 upon pressure release. This is based on Wright *et al*'s experimental observation [43] that there is no coordination change in permanently densified vitreous B_2O_3. In the present study, the coordination-dependent three-body potential is only used for O–B–O triplets, not for B–O–B triplets, and only 3 and 4-coordinated states are accounted for. The ⟨B–O–B⟩ angles are always constrained to the experimental value of 130°. The values of various parameters for boron oxide are also described in [42]. The cutoff for the Coulombic interaction is 10.6 Å, and for the short-range interaction between B–B, B–O and O–O is 3, 2 and 3 Å, respectively.

To simulate B_2O_3 glass, we started from the cesium enneaborate ($Cs_2O{\cdot}9B_2O_3$) crystal structure [44], which has both boroxol groups and triborate groups. After extracting Cs_2O and some BO_3 triplets, a unit cell of 80 atoms is obtained, which has 75% B atoms inside boroxol rings [45, 46]. MD simulations were carried out for 640-atom (256 B and 384 O) and 2560-atom (1024 B and 1536 O) systems with periodic boundary conditions to ascertain the absence of system size effects. These systems were heated up to 2500 K and equilibrated for different time periods, up to a nanosecond. Depending on the duration of equilibration, different amounts of boroxol rings dissolve and thus we were able to generate B_2O_3 melts with 75, 63 and 50 and 10% B atoms in the boroxol rings, respectively. These liquids are subsequently quenched at a rate of 2.5 K ps^{-1} and at constant pressure of 0.1 MPa to get initial glass samples. Temperature ramping was achieved by velocity rescaling, while the density was adjusted according to the Anderson constant-pressure algorithm [47]. Experiments show that the fraction of boroxol rings increases with decreasing temperature [48]. However, in MD simulations, no additional boroxol rings are generated with decreasing temperature. Part of the reason for this is the extremely high quench rate in MD simulations; the reactions that would have taken place on experimental timescales are simply suppressed. For systems with 10% to 75% boroxol rings, the density at ambient conditions ranges from 1.75 to 1.81 g cm^{-3}, respectively, very close to the experimental value of 1.80 g cm^{-3} for B_2O_3 glass [5]. In figures 1(a) and (b) we show that the total and partial structure factors $S(Q)$ of the sample with 63% boroxol rings, which, of all simulated systems show the best agreement with experimental data [9, 34, 43]. No remnants of the initial crystalline structure were found in glasses so prepared. However, since B_2O_3 liquids with different boroxol rings were equilibrated at 2500 K for different amounts of time before being quenched, the simulated configurations remain to a varying degree removed from equilibrium, the more so the higher the boroxol ring concentration. So no attempt is made to establish the relation between density and boroxol ring concentration of initial B_2O_3 glasses. Nevertheless, in this fashion B_2O_3 glasses with a wide range of boroxol ring concentrations can be generated in MD simulations, for which both density and structure factor closely reproduce experimental data.

The simulated hydrostatic compression–decompression cycles were carried out at 300 K by imposing pressures ranging from 0 to 50 GPa. To this end, the target pressure was

gradually ramped at a rate of 0.05 GPa ps^{-1}, while the system volume was allowed to adjust according to the Anderson constant-pressure algorithm. At intervals of 1 GPa, structures were further relaxed for a duration of 20 ps and statistical information was collected over 20 ps. The bulk modulus of B_2O_3 glass was calculated directly from the equation of state according to $B = \rho(\mathrm{d}P/\mathrm{d}\rho)$.

3. Results

The longitudinal and shear sound velocity as a function of pressure were previously measured in our Brillouin scattering experiments reported in [40]. In order to compare experimental data directly with MD simulation results, we have two choices. We can first convert the experimental sound velocities into bulk moduli, which requires knowledge of the density of B_2O_3 glass at each pressure. Unfortunately, it was not possible to determine this information in experiments with the required accuracy while the sample is enclosed in the diamond anvil cell. Alternatively, we can convert the simulated elastic moduli into sound velocities. The disadvantage of this approach is that we then end up comparing a composite quantity, given that the sound velocity is proportional to the square root of the modulus divided by the density. Such a comparison provides less insight, because the sudden drop in sound velocities at 2–3 GPa on decompression could be the result of a sudden change in the modulus or in the density. The first situation would reflect a second order transformation whereas the second situation would correspond to a first order transformation. In other words, the pressure dependence of the sound velocity does not reveal the nature of this transition. For the analysis presented here, we therefore pursue an approximate procedure for estimating the lower-bound density changes in the experiment and carry out a comparison on this basis.

From the pressure dependence of the longitudinal sound velocity V_p and shear sound velocity V_s, we know:

$$V_p = \sqrt{\frac{B + \frac{4}{3}G}{\rho}}, \tag{1}$$

$$V_s = \sqrt{\frac{G}{\rho}}, \tag{2}$$

where B, G and ρ are the bulk modulus, shear modulus and density, respectively. Eliminating the shear modulus, we get:

$$B = (V_p^2 - \tfrac{4}{3}V_s^2)\rho = V^2\rho, \tag{3}$$

where $V^2 = V_p^2 - \frac{4}{3}V_s^2$. Assuming that V is the properly reduced velocity of sound (i.e., a combination of longitudinal and shear velocities), such that $B = \rho\frac{\partial p}{\partial \rho} = V^2\rho$, the pressure dependence of the density then simplifies to:

$$\frac{\partial p}{\partial \rho} = V^2, \tag{4}$$

or

$$\partial\rho = \frac{1}{V^2}\partial p. \tag{5}$$

This represents the situation at a particular density. As the pressure changes, the density changes, and if it does so in a monotonous fashion we can expand the pressure–density relationship as a Taylor series,

$$\rho_1 = \rho_0 + \frac{\partial\rho_0}{\partial p}(p_1 - p_0) + \frac{1}{2}\frac{\partial^2\rho_0}{\partial p^2}(p_1 - p_0)^2 + \mathrm{O}(\Delta p^3). \tag{6}$$

Then taking the derivative of (6), we get:

$$\frac{\partial\rho_1}{\partial p} = \frac{\partial\rho_0}{\partial p} + \frac{\partial^2\rho_0}{\partial p^2}(p_1 - p_0) + \mathrm{O}(\Delta p^2), \tag{7}$$

where $\frac{\partial\rho_0}{\partial p} = \frac{1}{V_0^2}$ and $\frac{\partial\rho_1}{\partial p} = \frac{1}{V_1^2}$ are known from experiments, so we can solve for $\frac{\partial^2\rho_0}{\partial p^2}$ to yield:

$$\begin{aligned}\frac{\partial^2\rho_0}{\partial p^2} &= \frac{1}{(p_1 - p_0)}\left(\frac{\partial\rho_1}{\partial p} - \frac{\partial\rho_0}{\partial p}\right)\\ &= \frac{1}{(p_1 - p_0)}\left(\frac{1}{V_1^2} - \frac{1}{V_0^2}\right).\end{aligned} \tag{8}$$

Substituting (8) into (6) gives the corrected prediction of ρ_1:

$$\begin{aligned}\rho_1 &= \rho_0 + \frac{1}{V_0^2}(p_1 - p_0)\\ &\quad + \frac{1}{2}\frac{1}{(p_1 - p_0)}\left(\frac{1}{V_1^2} - \frac{1}{V_0^2}\right)(p_1 - p_0)^2 + \mathrm{O}(\Delta p^3)\\ &= \rho_0 + \frac{1}{2}\left(\frac{1}{V_1^2} + \frac{1}{V_0^2}\right)(p_1 - p_0) + \mathrm{O}(\Delta p^3).\end{aligned} \tag{9}$$

Given the initial density ρ_0, as well as V_0, V_1, p_0 and p_1 from the sound velocity versus pressure curves in experiments, we can obtain an estimate of the density and bulk modulus at each pressure. These are only estimates because in this procedure we ignore any amount of permanent densification, i.e., we assume that all deformation is elastic and therefore reversible. If permanent densification occurs, we underestimate the density.

From MD simulations we directly calculate the density and bulk modulus. We compare experimental and simulation results in figure 2. Regardless of the boroxol ring concentration, upon compression the density and bulk modulus smoothly increase in MD simulations, and upon decompression density and bulk modulus follow a different path, remaining higher and exhibiting less of pressure dependence. Upon decompression, the bulk modulus decreases smoothly until a transition occurs at about 2–3 GPa, upon which the bulk modulus returns to values followed during compression. Correspondingly, a marked change in slope is seen on the density curve at this pressure. In general terms these trends echo those observed in experiments.

There are, however, some differences that require further examination. For example, while a definite inflection around 3 GPa is apparent in the data, the drop in bulk modulus upon decompressing simulated structures may not appear as abrupt as the drop in sound velocity observed in experiments. Note that even on the timescale of the experiments, the distinctness of this drop in sound velocity depends on the decompression rate. The drop is only sharp if several hours of relaxation,

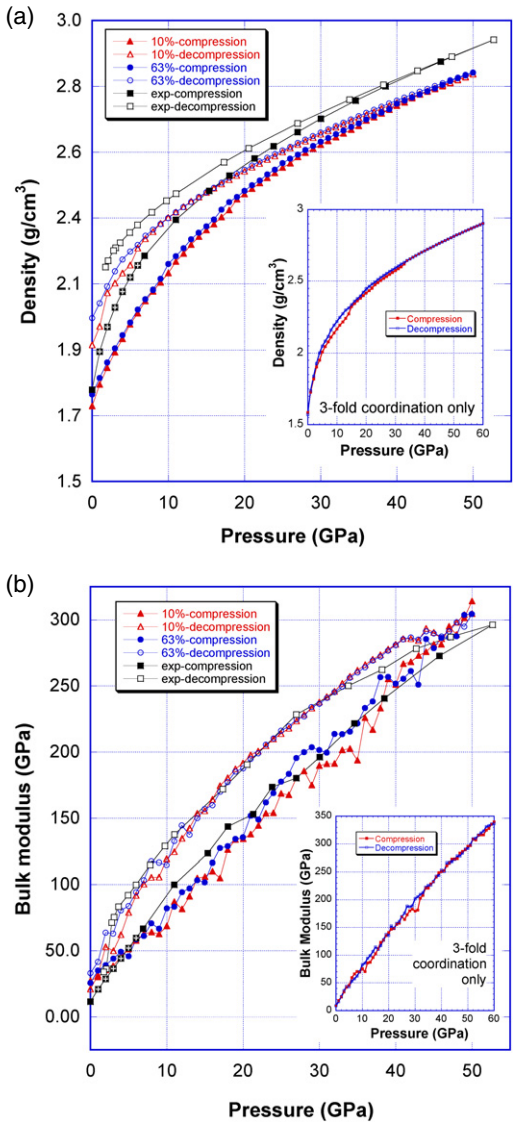

Figure 2. Comparison between MD simulated (samples with initially 10% and 63% boroxol rings at 300 K) and experimentally determined properties of vitreous B_2O_3 as a function of pressure during compression and decompression: (a) density; (b) bulk moduli. The insets in each figure show the simulation results obtained using an interaction potential that does not allow for boron to become 4-coordinated by oxygen. Squares with crosses inside indicate interpolated data (see text).

typically half a day, is allowed between successive pressure reductions; it is much more gradual if only minutes are provided. Since such extensive relaxation periods are not feasible in simulations, we cannot expect the transformation to be as sharp in simulations as in experiments. Furthermore, the density curves derived from experiments are shifted upwards with respect to those in MD simulations. This can possibly be attributed to several sources. We note that the experimental data are sparse in the low-pressure regime. In fact, one atmosphere velocities could not be measured on the actual samples compressed in the diamond cell. After mounting the glass sample in between the diamonds, the pressure in the anvil was already at 7.8 GPa, so that the first value of the sound velocity for this sample was measured at this pressure. Thus, the ambient pressure sound velocity had to be obtained from a different sample outside of the diamond anvil cell. It is therefore possible that, given somewhat different preparation histories, the ambient pressure sound velocity is lower than that of the sample that was used for the compression experiment. Low sound velocity means high compressibility and elastic volume change. Combined with the large first pressure increment, this would indeed result in a large initial error in the extrapolation procedure based on equation (9), and explain the systematic but virtually constant overestimation of the density. This argument is supported by the fact that beyond this initial stage, the density curves during compression and decompression in MD simulations are approximately parallel to their counterparts in experiments. To ameliorate the density overestimation, we generated velocity data in between zero and 7.8 GPa through interpolation. To this end we fitted the sound velocity versus pressure data over the entire pressure range using a polynomial. Sound velocity values were then evaluated from this polynomial for the desired pressure values (squares with open crosses in figure 2), thus achieving a discretization Δp sufficiently small to mitigate the error introduced by the procedure based on equation (9).

Upon computing the density change over a complete compression–decompression cycle of the experimental specimen, we find a permanent densification of about 20% at 1 bar for the recovered glass. Considering that the numerical procedure used to obtain this result actually neglects any non-elastic volume change, this represents the most conservative estimate of permanent densification. In reality it might actually be larger. Our simulations yield about 14% of residual densification, somewhat smaller, probably because of the limited time afforded by simulations for the structures to equilibrate while under pressure. At this point we can conclude that B_2O_3 glass undergoes irreversible structural changes upon compression that lead to a denser glass, unless a spontaneous spring-back of the specimen's volume occurred during the transition at which the sound velocities dropped. As shown in figure 2, MD simulations give us no such indication—they rather indicate that it is the elastic modulus that changes discontinuously, which makes this a second order transformation according to the Ehrenfest scheme.

4. Discussion

Based on the qualitative agreement between the pressure dependence of the modulus in experiment and simulation we can conclude that the key structural rearrangements in B_2O_3 glass under pressure are reproduced in our MD simulations. The analysis of the pertinent developments in our simulated structures is summarized in the following. Figure 3 shows that in B_2O_3 glass at ambient pressure boron is entirely three-coordinated, above 10 GPa an increasing number of boron is continuously converted to four-coordination upon densification. This is in good qualitative agreement with a very recent inelastic x-ray scattering study of vitreous B_2O_3 under pressure [41]. At the same time, the boroxol rings disintegrate, as shown in figure 4, which explains the disappearance of

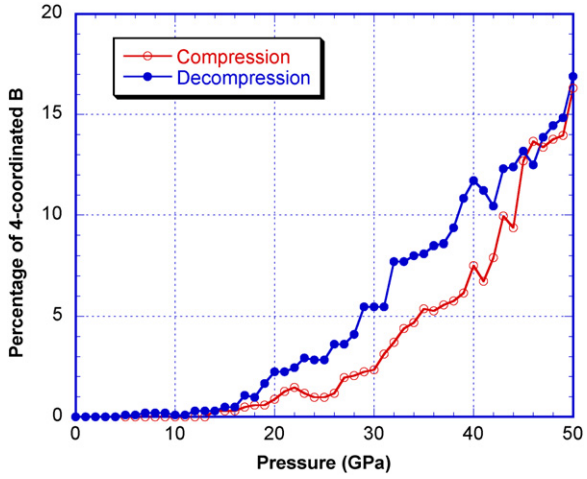

Figure 3. Percentage of 4-coordinated boron atoms as a function of pressure during the compression and decompression cycle at 300 K.

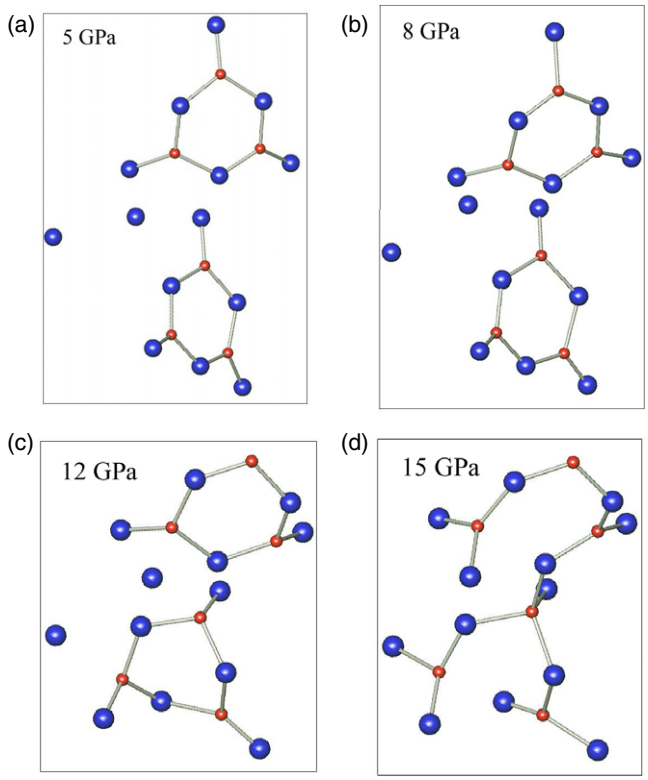

Figure 4. (a)–(d) show the disintegration of boroxol rings and the change of the coordination of boron from 3 to 4 upon increasing the pressure. (Small atoms are boron, the large ones are oxygen.)

the 808 cm^{-1} Raman line of the boroxol ring breathing mode under pressure in figure 5(a). Upon decompression, the percentage of four-coordinated boron follows the same path as during compression at very high pressures; then deviates from that path and maintains a higher value until the pressure reaches 16 GPa, and finally it returns to the compression curve. The continuous coordination conversion under pressure can be understood in terms of the structural disorder associated with the amorphous state of matter. Due to the fluctuations in the local stress fields, the coordination conversion occurs first at locations of highest stress intensity. Such a conversion to a more compact state relieves stress in the immediate surroundings, and subsequent transitions require further compression. This explains why the global properties of the glass structure only change gradually as a function of pressure. The gradual conversion of BO_3 triangles into denser BO_4 tetrahedra under pressure eventually eliminates most of the free volume in B_2O_3 glass [41, 49]. This densification is non-elastic, so that upon decompression it is improbable that the material would follow the same path of structural evolution as on compression. In fact, by entering into a state that includes BO_4 units at high pressures, the boron atoms easily end up

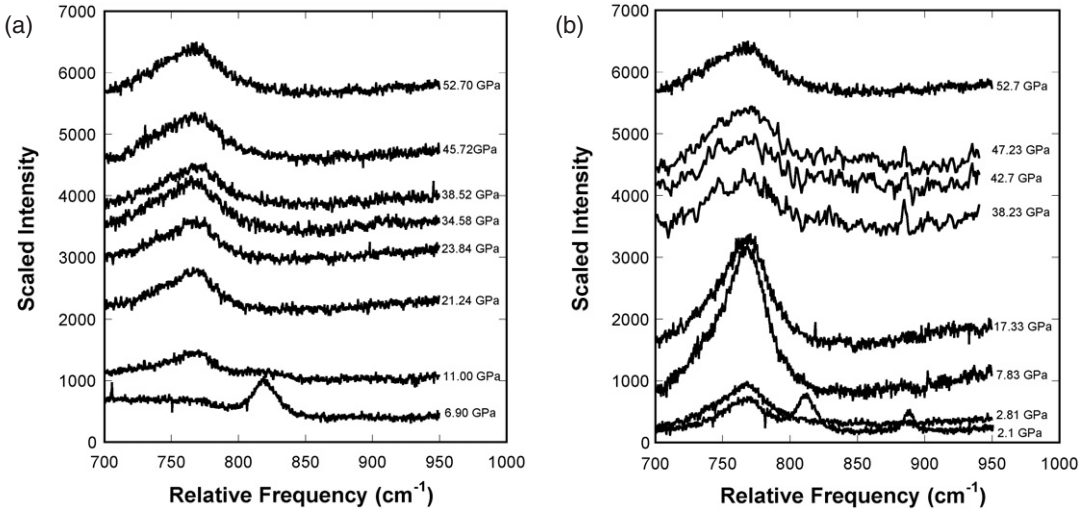

Figure 5. Stacked B_2O_3 Raman spectra during the experimental compression and decompression cycles. Raman spectra during compression (a) and decompression (b). The peak at 760 cm^{-1} is fluorescence from the diamond anvils, the peak at 812 cm^{-1} is the pressure-shifted boroxol ring mode, and the peak at 881 cm^{-1} is a previously unidentified Raman peak. The baseline of each spectrum has been shifted by an amount equal to 100 times the pressure at which the spectrum was collected. The number to the right of each spectrum is the pressure at which it was collected.

being bonded to completely different neighbors upon reversal of this coordination change. The structure of the recovered glass may have different ring size and ring shape. For example, while the re-emergence of the 808 cm^{-1} peak, albeit shifted to 812 cm^{-1}, suggests the recovery of boroxol rings, the new peak at 881 cm^{-1} could be attributed to trigonal B–$(OH)_3$ units [40] or to dipentaborate-like units [50, 51] that form upon decompression. Similar to experimental observations [41, 49], our study shows that there are no four-coordinated boron atoms in permanently densified B_2O_3 glass at one atmosphere. In other words, while under pressure B_2O_3 glass undergoes a reversible coordination transformation that results in an irreversible densification once pressure is released.

Unfortunately, it is not exactly known at what pressure the coordination conversion takes place during decompression in experiments [41]. If it is fully responsible for the sharp transition near 2–3 GPa upon decompression in experiments, then the coordination conversion in MD simulations occurs at higher pressure than in experiments. While we cannot completely exclude other reasons for this sharp transition at this moment, by argument of elimination our MD simulations do show that the coordination conversion under pressure plays a crucial role in polyamorphic transitions in B_2O_3 glass. Insets in figures 2(a) and (b) show that when using a three-body potential that does not allow for a coordination change, no permanent densification takes place even at 1000 K upon releasing from a maximum pressure of 60 GPa. The bulk modulus curves overlap with each other on compression and decompression, which is completely different from what is observed in experiments at 300 K. The above observations show that the polyamorphic transitions in three-coordinated B_2O_3 glass involve transitory four-coordinated boron atoms at high pressures, while coordination change is not necessary for compaction of four-coordinated silica glass. This may be true for all three-coordinated glasses and four-coordinated glasses, respectively.

Despite going through a coordination change under pressure, the short- and intermediate-range structure in permanently densified three-coordinated glass evolves in a fashion comparable to that of four-coordinated glasses. Similar to what we observed in silica glass [35, 36], not much change is seen between the short-range order of the recovered and original B_2O_3 glass, as revealed by the radial distribution functions, bond angle distributions as well as coordination states, which is consistent with the experimental findings of Wright *et al* [43]. The uniqueness of the short-range order in the densified glass was further verified in our experiments by the fact that we could loop the sound velocity versus pressure cycle multiple times. However, the intermediate-range order is substantially more affected by pressure-induced structural modifications than the short-range order, which is manifest in the ring size distribution in the initial and recovered glass in figure 6. The number of large rings increases significantly in the densified structure in comparison to the original glass. In vitreous B_2O_3, this is accomplished by going through the transient four-coordinated states at high pressures, while in silica glass it is simply achieved by swapping neighbors without the involvement of the high-coordinated states. Nevertheless, the increase of large rings facilitates the permanent densification in both systems.

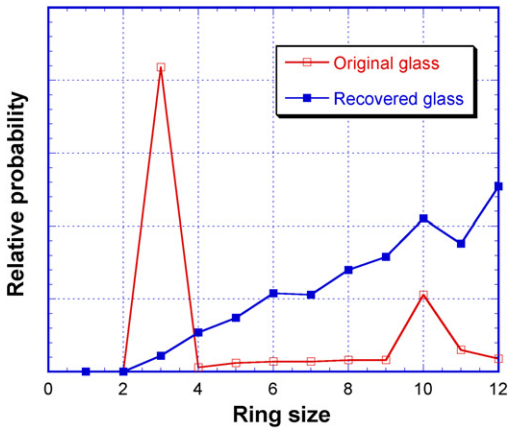

Figure 6. Ring size distribution in original and recovered B_2O_3 glass.

Our simulations show that the concentration of boroxol rings has a relatively small effect on the magnitude and pressure dependence of density and bulk modulus of the simulated glasses. The density of as-quenched glasses vary depending on the time allowed for equilibration at high temperatures. However, this difference diminishes quickly upon compression, partly due to the different compliances of these structures and, more significantly, because boroxol rings disintegrate with increasing pressure. The influence of boroxol rings on the elastic properties is even less pronounced. These small rings appear to contribute little to the overall load bearing capacity of the network, and once they disintegrate upon compression, the network approaches a similar topology independent of the starting concentration of boroxol rings. Note that in our simulations, boroxol rings disintegrate rather precipitously once pressure exceeds about 8–10 GPa. Figure 6 also shows that in simulations boroxol rings cannot regenerate during decompression, which is different from the experimental observation that at the completion of the transition near 2 GPa, the 808 cm^{-1} boroxol ring mode suddenly reappears during decompression, indicating the reformation of boroxol rings in the recovered glass in figure 5(b). This, we believe, is partially because the simulated glass is not relaxed on the experimental timescale. Wright *et al* [43] have shown that B_2O_3 glass can relax at ambient conditions, and it takes days for the fraction of boroxol rings to return to its original value after pressurization. In future work, the forces necessary to account for the 6.4 kcal mol^{-1} boroxol ring stabilization energy observed by Walrafen *et al* [52] may have to be included explicitly in the interaction model, in order to easily generate boroxol rings in initial and recovered B_2O_3 glass.

5. Conclusions

Using the newly developed coordination-dependent charge transfer potential, we observed polyamorphic transitions in vitreous boron oxide under pressure in MD simulations that

correspond well to those observed in Brillouin scattering experiments. Our MD simulations show that a transient coordination conversion is requisite to achieve a pressure-induced permanent densification of three-coordinated B_2O_3 glass, while this is not necessary for the irreversible compaction of four-coordinated silica glass. The boroxol rings in simulated vitreous B_2O_3 break up when subject to pressure, which is in accordance with the disappearance of the breathing mode in the experimental Raman spectrum of B_2O_3 glass under pressure. While boroxol rings do not regenerate upon pressure release on the short timescales characteristic of MD simulations, an overall shift of the ring size distribution towards larger rings characterizes the structural changes in the permanently densified B_2O_3 glass, which in experiments are evident through a new peak in the Raman spectrum. The sudden drop in the sound velocities observed in experiment is likely the signature of a second order structural transition.

Acknowledgments

The authors acknowledge the support of the National Institute of Standards and Technology under Grant No. 60NANB9D0102, Saint-Gobain Recherche, and the National Science Foundation under Grant Nos DMR-0072258 and EAR-0135642. Most of the computational work was done on super-computers in the Center for Advanced Computing (CAC) at the University of Michigan. L Huang would like to thank Dr Linn Hobbs in MIT for stimulating discussions. The authors would also like to thank S Sinogeikin for technical assistance with the original Brillouin experiments.

References

[1] Zachariasen W H 1932 *J. Am. Chem. Soc.* **54** 3841
[2] Warren B E, Krutter H and Morninstar O 1936 *J. Am. Ceram. Soc.* **19** 202
[3] Svanson S E and Johansso R 1969 *Acta Chem. Scand.* **23** 635
[4] Fajans K and Barber S W 1952 *J. Am. Chem. Soc.* **74** 2761
[5] Johnson P A V, Wright A C and Singlair R N 1982 *J. Non-Cryst. Solids* **50** 281
[6] Goubeau J and Keller H 1953 *Z. Anorg. Allg. Chem.* **272** 303
[7] Krogh-Moe J 1969 *J. Non-Cryst. Solids* **1** 269
[8] Galeener F L 1982 *Solid State Commun.* **44** 1037
[9] Mozzi R L and Warren B E 1970 *J. Appl. Crystallogr.* **3** 251
[10] Hannon A C, Grimley D I, Hulme R A, Wright A C and Sinclair R N 1994 *J. Non-Cryst. Solids* **177** 299
[11] Sinclair R N, Stone C E, Wright A C, Polyakova I G, Vedishcheva N M, Shakhmatkin B A, Feller S A, Johanson B C, Venhuizen P, William R B and Hannon A C 2000 *Phys. Chem. Glasses* **41** 286
[12] Jellison G E, Panek L W, Bray P J and Rouse G B 1977 *J. Chem. Phys.* **66** 802
[13] Joo C, Werner-Zwanziger U and Zwanziger J W 2000 *J. Non-Cryst. Solids* **261** 282
[14] Walrafen G E, Chu Y C and Hokmabadi M S 1990 *J. Chem. Phys.* **92** 6987
[15] Dunlevey F M and Cooper A R 1977 *Structure of Non-Crystalline Materials* ed P H Gaskell (London: Taylor and Francis)
[16] Soppe W, van der Marela C, van Gunsteren W F and den Hartog H W 1988 *J. Non-Cryst. Solids* **103** 201
[17] Wright A C, Sumner D J and Clare A G 1982 *The Structure of Non-Crystalline Materials* ed P H Gaskell (New York: Taylor and Francis)
[18] Williams S J and Elliott S R 1982 *The Structure of Non-Crystalline Materials* ed P H Gaskell (New York: Taylor and Francis)
[19] Elliott S R 1978 *Phil. Mag.* B **37** 435
[20] Soppe W and den Hartog H W 1988 *J. Phys. C: Solid State Phys.* **21** L689
[21] Soppe W and den Hartog H W 1989 *J. Non-Cryst. Solids* **108** 260
[22] Xu Q, Kawamura K and Yokokawa T 1988 *J. Non-Cryst. Solids* **104** 261
[23] Verhoef A H and den Hartog H W 1991 *Radiat. Eff. Defects Solids* **119–121** 493
[24] Verhoef A H and den Hartog H W 1992 *J. Non-Cryst. Solids* **146** 267
[25] Verhoef A H and den Hartog H W 1994 *J. Non-Cryst. Solids* **180** 102
[26] Inoue H, Aoki N and Yasui I 1987 *J. Am. Ceram. Soc.* **70** 622
[27] Takada A, Catlow C R A and Price G D 1995 *J. Phys.: Condens. Matter* **7** 8693
[28] Youngman R E, Kieffer J, Bass J D and Duffrène L 1997 *J. Non-Cryst. Solids* **222** 190
[29] Fernández-Perea R, Bermejo F J and Enciso E 1996 *Phys. Rev.* B **53** 6215
[30] Fernández-Perea R, Bermejo F J and Senent M L 1996 *Phys. Rev.* B **54** 6039
[31] Maranas J K, Chen Y Z, Stillinger D K and Stillinger F H 2001 *J. Chem. Phys.* **115** 6578
[32] Teter M 1996 *Proc. 2nd Int. Conf. on Borate Glasses, Crystals, and Melts* (Abingdon, UK: Society of Glass Technology)
[33] Swenson J and Börjesson L 1997 *Phys. Rev.* B **55** 11138
[34] Suzuya K, Yoneda Y, Kohara S and Umesaki N 2000 *Phys. Chem. Glasses* **41** 282
[35] Huang L P and Kieffer J 2004 *Phys. Rev.* B **69** 224203
[36] Huang L P and Kieffer J 2004 *Phys. Rev.* B **69** 224204
[37] Grimsditch M, Bhadra R and Meng Y 1988 *Phys. Rev.* B **38** 7836
[38] Nicholas J D, Youngman R E, Sinogeikin S V, Bass J D and Kieffer J 2003 *Phys. Chem. Glasses* **44** 249
[39] Nicholas J D, Sinogeikin S V, Kieffer J and Bass J D 2004 *J. Non-Cryst. Solids* **349** 30
[40] Nicholas J D, Sinogeikin S V, Kieffer J and Bass J D 2004 *Phys. Rev. Lett.* **92** 215701
[41] Lee S K, Eng P J, Mao H K, Meng Y, Newville M, Hu M Y and Shu J F 2005 *Nat. Mater.* **4** 851
[42] Huang L P and Kieffer J 2006 *Phys. Rev.* B **74** 224107
[43] Wright A C, Stone C E, Sinclair R N, Umesaki N, Kitamura N, Ura K, Ohtori N and Hannon A C 2000 *Phys. Chem. Glasses* **41** 296
[44] Krogh-Moe J and Ihara M 1967 *Acta Crystallogr.* **23** 427
[45] Takada A, Catlow C R A and Price G D 2003 *Phys. Chem. Glasses* **44** 147
[46] Takada A 2004 *Phys. Chem. Glasses* **45** 156
[47] Andersen H C 1980 *J. Chem. Phys.* **72** 2384
[48] Hassan A K, Torell L M, Börjesson L and Doweidar H 1992 *Phys. Rev.* B **45** 12797
[49] Lee S K, Mibe K, Fei Y W, Cody G D and Mysen B O 2005 *Phys. Rev. Lett.* **94** 165507
[50] Akagi R, Ohtori N and Umesaki N 2001 *J. Non-Cryst. Solids* **293** 471
[51] Iliescu T, Ardelean I and Simon S 1994 *Solid State Commun.* **90** 507
[52] Walrafen G E, Samanta S R and Krishnan P N 1980 *J. Chem. Phys.* **72** 113